Pergamon

PII: S0045-7949(96)00349-5

Computers & Structures Vol. 63, No. 2, pp. 203–216, 1997

0045-7949/97 $17.00 + 0.00

THE VIBRATION OF A RECTANGULAR LAMINATED ELASTIC PLATE WITH EMBEDDED PIEZOELECTRIC SENSORS AND ACTUATORS

R. C. Batra and **X. Q. Liang**

Department of Engineering Science & Mechanics, Virginia Polytechnic Institute and State University, Blacksburg, VA 24061-0219, U.S.A.

(*Received* 7 *December* 1995)

Abstract—We use the three-dimensional linear theory of elasticity to analyse the steady-state vibrations of a simply-supported rectangular linear elastic laminated plate with embedded PZT layers. Some of these PZT layers act as actuators while the remaining act as sensors. It is assumed that there is perfect bonding between different layers. Numerical results for a thin and a thick plate containing one embedded actuator layer and one embedded sensor layer are presented. For the former case, the optimum location of the centroid of the excited rectangular region that will result in the maximum out-of-plane displacement for a given distribution of the applied voltage is also determined. Equivalently, an equal and opposite voltage applied to this region of a vibrating plate will be most effective in diminishing these vibrations. The maximum shear stress at the interface between the sensor and the lamina is lower than that between the actuator and the lamina. The point of maximum output voltage from the sensor coincides with that of peak out-of-plane displacement. The variations of displacement and stress components through the thickness for the thin and thick plates are similar.

INTRODUCTION

An interesting problem in smart structures is to control the shape of a plate subjected to an external disturbance with the least expenditure of energy and/or in the least amount of time. It requires finding the optimum shapes, number and placement of actuators and sensors on a given plate and the design of a robust control algorithm [1, 2]. This general problem is hard to analyse, so we consider the following problem. Assume that a simply-supported rectangular laminated plate with thin piezoelectric layers embedded in it is vibrating freely at a frequency close to one of its natural freqencies. Find the optimum location and size of the rectangular region that should be excited with a minimum voltage represented by a half-sinusoidal wave on the excited region so that the motion of the plate is suppressed. We use the three-dimensional linear theory of elasticity to analyse this problem for the first few modes of vibration of the plate. We also compare the distributions of deformation fields and stresses in a thin and a thick plate. We note that a similar problem when PZT layers are fixed to the top and bottom surfaces of the plate has recently been analysed by Batra *et al.* [3]. However, the problem with embedded PZT layers is more practical since insulation from environmental effects, aesthetics and other design considerations may necessitate that PZT layers be embedded in the structure. Mathematically, the problem is more challenging because of (i) the additional effects involved in the equations of motion for the PZT layers; and (ii) the need to solve for the voltage output from PZTs used as sensors. Also more than one layer of PZT sensors and actuators can be embedded in the plate. As before [3], the PZT layers are modeled as thin films. Here, we also compare results for a thin and a thick plate.

Piezoelectric elements have been extensively used to control the vibrations of a beam, e.g. see Baz and Poh [4], Tzou and Tseng [5], and Crawley and de Luis [6]. Elastic plates with PZT films attached to their surfaces have been analyzed by using approximate two-dimensional plate theories [7–11], and also by using the three-dimensional equations of elasticity and the method of Fourier series [12–19]. Here we use the three-dimensional equations of linear elasticity to study the vibrations and structural response of a steadily vibrating simply-supported rectangular laminated plate.

FORMULATION OF THE PROBLEM

Governing equations

We consider a simply-supported rectangular laminated elastic plate of dimensions a and b in x_1 and x_2 directions, respectively. The total thickness of the plate made up of N layers, not necessarily of the same thickness and including N_s layers of sensors and N_a layers of actuators equals $2h$ (Fig. 1); the ith layer is determined by $h^{(i-1)} \leqslant x_3 \leqslant h^{(i)}$. We note that some of these layers are made of a linear piezoelectric material while others are made of a linear elastic material. Both sensors and actuators are modeled as thin films [20, 21] poled in the

x_3-direction, and are assumed to be transversely isotropic with x_3-axis as the preferred direction. Each of the elastic laminate is assumed to be made of an orthotropic material with constitutive equations given by

$$\tau_{\alpha\beta}^{(i)} = c_{\alpha\beta;\delta}^{(i)} e_{;\delta}^{(i)}, \quad \alpha, \beta, \gamma, \delta = 1, 2, 3,$$

$$e_{\alpha\beta}^{(i)} = (u_{\alpha,\beta}^{(i)} + u_{\beta,\alpha}^{(i)})/2. \tag{1}$$

Here $\tau_{\alpha\beta}$ is the Cauchy stress tensor, $c_{\alpha\beta;\delta}$ the material elasticity tensor, $e_{\alpha\beta}$ the infinitesimal strain tensor, u_a the displacement of a point, $u_{\alpha,\beta} = \partial u_\alpha/\partial x_\beta$, a repeated index implies summation over the range of the index, and a superscript i in parentheses indicates quantities for the ith layer. Henceforth we drop the superscript i unless it is needed for clarity.

For an elastic laminate, governing equations in terms of displacement $\mathbf{u}$ are

$$c_{11}^{(i)}u_{1,11}^{(i)} + c_{66}^{(i)}u_{1,22}^{(i)} + c_{55}^{(i)}u_{1,33}^{(i)} + (c_{12}^{(i)} + c_{66}^{(i)})u_{2,12}^{(i)} + (c_{13}^{(i)} + c_{55}^{(i)})u_{3,13}^{(i)} = \rho^{(i)}\ddot{u}_1^{(i)}$$

$$(c_{12}^{(i)} + c_{66}^{(i)})u_{1,12}^{(i)} + c_{66}^{(i)}u_{2,11}^{(i)} + c_{22}^{(i)}u_{2,22}^{(i)} + c_{44}^{(i)}u_{2,33}^{(i)} + (c_{23}^{(i)} + c_{44}^{(i)})u_{3,23}^{(i)} = \rho^{(i)}\ddot{u}_2^{(i)}$$

$$(c_{13}^{(i)} + c_{55}^{(i)})u_{1,13}^{(i)} + (c_{23}^{(i)} + c_{44}^{(i)})u_{2,23}^{(i)} + c_{55}^{(i)}u_{3,11}^{(i)} + c_{44}^{(i)}u_{3,22}^{(i)} + c_{33}^{(i)}u_{3,33}^{(i)} = \rho^{(i)}\ddot{u}_3^{(i)}$$

where a superimposed dot indicates material time derivative which for infinitesimal deformations reduces to partial time derivative, and $c_{\alpha\beta}$ are the material elasticities when $\tau_{\alpha\beta}$ and $e_{\alpha\beta}$ are written as six-dimensional vectors. The boundary conditions at the simply-supported edges, when the plate is viewed as a three-dimensional body, are

$$\tau_{11}^{(i)} = c_{11}^{(i)}u_{1,1}^{(i)} + c_{12}^{(i)}u_{2,2}^{(i)} + c_{13}^{(i)}u_{3,3}^{(i)} = 0,$$

$$u_3^{(i)} = 0, \quad u_2^{(i)} = 0 \quad \text{at} \quad x_1 = 0, \quad a$$

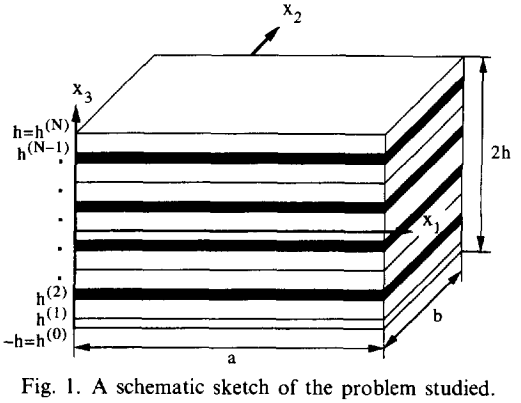

Fig. 1. A schematic sketch of the problem studied.

$$\tau_{22}^{(i)} = c_{12}^{(i)}u_{1,1}^{(i)} + c_{22}^{(i)}u_{2,2}^{(i)} + c_{23}^{(i)}u_{3,3}^{(i)} = 0,$$

$$u_3^{(i)} = 0, \quad u_1^{(i)} = 0 \quad \text{at} \quad x_2 = 0, \quad b. \tag{2}$$

These simulate a simply-supported edge characterized by the vanishing of the deflection and the bending moment there, and have been used by Srinivas *et al.* [15], Wittrick [16], and Yang *et al.* [18].

At the interface $x_3 = h^{(i)}$ between the ith and the $(i+1)$th layers, coherency conditions, i.e. the continuity of surface tractions and displacements, imply the following:

$$c_{55}^{(i)}(u_{3,1}^{(i)} + u_{1,3}^{(i)}) = c_{55}^{(i+1)}(u_{3,1}^{(i+1)} + u_{1,3}^{(i+1)}) \quad \text{at} \quad x_3 = h^{(i)}$$

$$c_{44}^{(i)}(u_{2,3}^{(i)} + u_{3,2}^{(i)}) = c_{44}^{(i+1)}(u_{2,3}^{(i+1)} + u_{3,2}^{(i+1)}) \quad \text{at} \quad x_3 = h^{(i)}$$

$$c_{13}^{(i)}u_{1,1}^{(i)} + c_{23}^{(i)}u_{2,2}^{(i)} + c_{33}^{(i)}u_{3,3}^{(i)} = c_{13}^{(i+1)}u_{1,1}^{(i+1)} + c_{23}^{(i+1)}u_{2,2}^{(i+1)} + c_{33}^{(i+1)}u_{3,3}^{(i+1)} \quad \text{at} \quad x_3 = h^{(i)}$$

$$u_1^{(i)} = u_1^{(i+1)}, \quad u_2^{(i)} = u_2^{(i+1)}, \quad u_3^{(i)} = u_3^{(i+1)} \quad \text{at} \quad x_3 = h^{(i)}. \tag{3}$$

Since the bottom and top surfaces of the plate are traction free, boundary conditions on them correspond to the vanishing of expressions on the left-hand sides of eqn (3) with $i = 1$, $x_3 = -h$ and $i = N$, $x_3 = h$, respectively.

Recalling that sensors and actuators are modeled as thin films, the balance of linear momentum and the Maxwell equation for any one of them can be written as [21]

$$\tau_{11,1}^{(i)} + \tau_{12,2}^{(i)} + [\![\tau_{31}^{(i)}]\!] = \rho^{(i)}\ddot{u}_1^{(i)},$$

$$\tau_{21,1}^{(i)} + \tau_{22,2}^{(i)} + [\![\tau_{32}^{(i)}]\!] = \rho^{(i)}\ddot{u}_2^{(i)},$$

$$[\![\tau_{33}^{(i)}]\!] = \rho^{(i)}\ddot{u}_3^{(i)},$$

$$D_{\alpha,\alpha}^{(i)} = 0, \tag{4}$$

where

$$[\![\tau_{31}^{(i)}]\!] = (\tau_{31}^{(i+1)}|_{x_3 = h^{(i)}} - \tau_{31}^{(i-1)}|_{x_3 = h^{(i-1)}})/h^{(i)},$$

and D_α is the electric displacement. The constitutive equations for a linear piezoelectric medium are

$$\mathbf{D} = \mathbf{e}^{\mathrm{T}}\mathbf{s} + \boldsymbol{\epsilon}\mathbf{E}$$

$$\boldsymbol{\tau} = \mathbf{c}\mathbf{s} - \mathbf{e}\mathbf{E}, \tag{5}$$

where $\mathbf{E}$ is the electric field vector given by $\mathbf{E} = -\operatorname{grad}\phi$, ϕ is the voltage field, $\mathbf{e}$ the piezoelectric constants and $\boldsymbol{\epsilon}$ the dielectric permittivity. We note that the material response of PZT and PVDF can be represented by constitutive eqn (5).

Since the thickness of a sensor or an actuator is very small as compared to that of a lamina, it is

reasonable to assume that $|D_{1,1}| \ll |D_{3,3}|$ and $|D_{2,2}| \ll |D_{3,3}|$ [20]. Thus eqn $(4)_4$ reduces to

$$D_{3,3}^{(i)} = 0, \quad \text{or} \quad \phi_{,33}^{(i)} = 0. \tag{6}$$

Following Brooks and Heyliger [14], we assume the electric potential ϕ to be a linear function of x_3. That is,

$$\phi^{(i)}(x_1, x_2, x_3, t) = \Phi^{(i)}(x_1, x_2, t)\frac{x_3 - h^{(i-1)}}{h^{(i)} - h^{(i-1)}}. \tag{7}$$

Hence eqn (6) or equivalently $(4)_4$ is identically satisfied.

Boundary conditions at the edges of a PZT sensor/actuator and at the interfacial surfaces are

$$\begin{aligned}
&\tau_{11}^{(i)} = u_2^{(i)} = u_3^{(i)} = 0, \quad \text{at} \quad x_1 = 0, \quad a,\\
&\tau_{22}^{(i)} = u_1^{(i)} = u_3^{(i)} = 0, \quad \text{at} \quad x_2 = 0, \quad b,\\
&u_\alpha^{(i)} = u_\alpha^{(i+1)}, \quad \text{at} \quad x_3 = h^{(i)},\\
&u_\alpha^{(i)} = u_\alpha^{(i-1)}, \quad \text{at} \quad x_3 = h^{(i-1)}.
\end{aligned} \tag{8}$$

Note that the continuity of tractions at the interface between the piezoelectric layer and the lamina has been considered in writing the equations of motion for a piezoelectric material point. For an actuator, we also have

$$\Phi^{(i)}(x_1, x_2, t) = \begin{cases} V^a(x_1, x_2, t) & \text{at} \quad x_3 = h^{(i)}, \\ 0 & \text{at} \quad x_3 = h^{(i-1)}, \end{cases} \tag{9}$$

and for a sensor,

$$\begin{aligned}
&\Phi^{(i)}(x_1, x_2, t) = 0 \quad \text{at} \quad x_3 = h^{(i-1)},\\
&D_3 = 0 \quad \text{at} \quad x_3 = h^{(i)}.
\end{aligned} \tag{10}$$

This completes the formulation of the problem.

Time harmonic vibrations

We assume that the actuators are excited by a time harmonic voltage

$$V^{(i)}(x_1, x_2, t) = \tilde{V}^{(i)}(x_1, x_2)e^{i\omega t}, \tag{11}$$

and seek solutions of the governing equations which are also time harmonic with the same frequency. That is

$$\begin{aligned}
&u_\alpha^{(i)}(x_1, x_2, x_3, t) = \tilde{u}_\alpha^{(i)}(x_1, x_2, x_3)e^{i\omega t},\\
&\Phi^{(i)}(x_1, x_2, t) = \tilde{\Phi}^{(i)}(x_1, x_2)e^{i\omega t}.
\end{aligned} \tag{12}$$

Henceforth we drop the superimposed tilde. The form of equations given in the preceding section is unchanged except that $\ddot{\mathbf{u}}$ is replaced by $-\omega^2\mathbf{u}$.

SOLUTIONS

The solution procedure is similar to that described by Yang *et al.* [19] and is therefore briefly sketched below.

Solutions for the substrate laminates

We assume that the displacements of the ith layer can be represented by the following Fourier series.

$$\begin{aligned}
u_1^{(i)} &= \sum_{m,n=1}^{\infty} a_{1mn}^{(i)}(x_3)\cos\alpha_m x_1 \sin\beta_n x_2\\
u_2^{(i)} &= \sum_{m,n=1}^{\infty} a_{2mn}^{(i)}(x_3)\sin\alpha_m x_1 \cos\beta_n x_2\\
u_3^{(i)} &= \sum_{m,n=1}^{\infty} a_{3mn}^{(i)}(x_3)\sin\alpha_m x_1 \sin\beta_n x_2
\end{aligned}$$

$$\alpha_m = m\pi/a, \quad \beta_n = n\pi/b. \tag{13}$$

These satisfy boundary conditions at the edges $x_1 = 0, a$ and $x_2 = 0, b$. Substitution of (13) into the governing equations obtained from (1) and $(12)_1$ yields ordinary differential equations for $a_{\alpha mn}(x_3)$ which are solved by assuming that

$$a_{\alpha mn}(x_3) = A_{\alpha mn}\, e^{\eta_{mn}x_3}, \quad \text{no sum on } m, n, \tag{14}$$

where $A_{\alpha mn}$ are undetermined constants. Equation (14) when substituted into the ordinary differential equations will yield a set of linear homogeneous equations for the determination of $A_{\alpha mn}$; the coefficients of these equations involve the elastic constants for the material of the laminate and the frequency ω. In order for these equations to have a nontrivial solution, the determinant of the coefficients of $A_{\alpha mn}$ must vanish. This gives the following cubic equation for $(\eta_{mn})^2$.

$$(\eta_{mn})^6 + a(\eta_{mn})^4 + b(\eta_{mn})^2 + c = 0. \tag{15}$$

Explicit expressions for a, b and c in terms of the elasticities of the laminate and the frequency ω are given in Yang *et al.* [19]. For distinct real or complex conjugate roots η_{mnp}, $p = 1, 2, \ldots, 6$, we have

$$a_{\alpha mn}(x_3) = D_{mnp}F_{\alpha mnp}\, e^{\eta_{mnp}x_3}$$

no sum on m, n, but summed on p (16)

where D_{mnp} is an arbitrary constant and $F_{\alpha mnp}$ is a function of η_{mnp} and the material parameters. We note that for a few values of ω, eqn (15) may have repeated real roots; it is more likely to occcur for an isotropic material. We exclude those special values of ω.

Equation (16) when substituted into (13) gives the displacement field in the ith laminate.

$$u_1^{(i)} = \sum_{m,n=1}^{\infty} \left[\sum_{p=1}^{6} D_{mnp}^{(i)} F_{1mnp}^{(i)}(x_3) \right] \cos \alpha_m x_1 \sin \beta_n x_2,$$

$$u_2^{(i)} = \sum_{m,n=1}^{\infty} \left[\sum_{p=1}^{6} D_{mnp}^{(i)} F_{2mnp}^{(i)}(x_3) \right] \sin \alpha_m x_1 \cos \beta_n x_2,$$

$$u_3^{(i)} = \sum_{m,n=1}^{\infty} \left[\sum_{p=1}^{6} D_{mnp}^{(i)} F_{3mnp}^{(i)}(x_3) \right] \sin \alpha_m x_1 \sin \beta_n x_2. \quad (17)$$

Thus strains and stresses in the ith laminate can be computed. The continuity conditions at the interface $x_3 = h^{(i)}$ between the two laminates yield

$$[D_{mnp}^{(i)}] = [T^{(i)}][D_{mnp}^{(i+1)}] \quad (18)$$

where $[D_{mnp}^{(i)}]$ is a 6×1 matrix (for $p = 1, 2, \ldots, 6$) and $[T^{(i)}]$ is a 6×6 matrix whose elements are functions of $F_{\alpha mnp}^{(i)}$ and $F_{\alpha mnp}^{(i+1)}$ evaluated at $x_3 = h^{(i)}$. Equation (18) is a recursive relation between constants for the ith and $(i+1)$th laminate and can be used repeatedly to express constants for the kth laminate in terms of those for the lth laminate provided that no sensor or actuator layer is between them.

The traction-free conditions at the top and bottom surfaces yield

$$\sum_{p=1}^{6} R_{\alpha mnp}^{(1)} D_{mnp}^{(1)} = 0, \quad \sum_{p=1}^{6} R_{\alpha mnp}^{(N)} D_{mnp}^{(N)} = 0, \quad (19)$$

where $R_{\alpha mnp}^{(1)}$ and $R_{\alpha mnp}^{(N)}$ are functions of $F_{\alpha mnp}^{(N)}$ evaluated at $x_3 = -h$ and $x_3 = h$, respectively.

Solutions for actuator layers

For the ith-layer made of a PZT material and assumed to act as an actuator, we presume that

$$u_1^{(i)}(x_1, x_2) = \sum_{m,n=1}^{\infty} \bar{D}_{1mn}^{(i)} \cos \alpha_m x_1 \sin \beta_n x_2,$$

$$u_2^{(i)}(x_1, x_2) = \sum_{m,n=1}^{\infty} \bar{D}_{2mn}^{(i)} \sin \alpha_m x_1 \cos \beta_n x_2,$$

$$u_3^{(i)}(x_1, x_2) = \sum_{m,n=1}^{\infty} \bar{D}_{3mn}^{(i)} \sin \alpha_m x_1 \sin \beta_n x_2 \quad (20)$$

where

$$\bar{D}_{1mn}^{(i)} = \frac{4}{ab} \int_0^a \int_0^b u_1^{(i)} \cos \alpha_m x_1 \sin \beta_n x_2 \, dx_1 \, dx_2 \quad (21)$$

and similar expressions hold for $\bar{D}_{2mn}^{(i)}$ and $\bar{D}_{3mn}^{(i)}$. These satisfy the homogeneous edge conditions $(8)_{1,2}$. In order to avoid term by term differentiation and to take care of the nonhomogeneous boundary conditions (9) at the same time, we multiply equations obtained from $(4)_{1-3}$ by $\cos \alpha_m x_1 \sin \beta_n x_2$, $\sin \alpha_m x_1 \cos \beta_n x_2$ and $\sin \alpha_m x_1 \sin \beta_n x_2$, respectively, and integrate the resulting equations over $0 < x_1 < a$ and $0 < x_2 < b$. With integration by parts and the use of boundary conditions we arrive at the following.

$$\sum_{p=1}^{6} R_{mnp}^{(i+1)}(h^{(i)}) D_{mnp}^{(i+1)} - \sum_{p=1}^{6} R_{mnp}^{(i-1)}(h^{(i-1)}) D_{mnp}^{(i-1)}$$

$$+ h^{(i)}(\rho^{(i)}\omega^2 - c_{11}^{(i)}\alpha_m^2 - c_{66}^{(i)}\beta_n^2)\bar{D}_{1mn}^{(i)}$$

$$- h^{(i)}(c_{12}^{(i)} + c_{66}^{(i)})\alpha_m \beta_n \bar{D}_{2mn}^{(i)}$$

$$= -\frac{4e_{31}^{(i)}}{ab} \alpha_m \int_0^a \int_0^b \tilde{V}^{(i)} \sin \alpha_m x_1 \sin \beta_n x_2 \, dx_1 \, dx_2,$$

$$\sum_{p=1}^{6} Q_{mnp}^{(i+1)}(h^{(i)}) D_{mnp}^{(i+1)} - \sum_{p=1}^{6} Q_{mnp}^{(i-1)}(h^{(i-1)}) D_{mnp}^{(i-1)}$$

$$- h^{(i)}(c_{12}^{(i)} + c_{66}^{(i)})\alpha_m \beta_n \bar{D}_{1mn}^{(i)}$$

$$+ h^{(i)}(\rho^{(i)}\omega^2 - c_{66}^{(i)}\alpha_m^2 - c_{11}^{(i)}\beta_n^2)\bar{D}_{2mn}^{(i)}$$

$$= -\frac{4e_{31}^{(i)}}{ab} \beta_n \int_0^a \int_0^b \tilde{V}^{(i)} \sin \alpha_m x_1 \sin \beta_n x_2 \, dx_1 \, dx_2,$$

$$\sum_{p=1}^{6} P_{mnp}^{(i+1)}(h^{(i)}) D_{mnp}^{(i+1)} - \sum_{p=1}^{6} P_{mnp}^{(i-1)}(h^{(i-1)}) D_{mnp}^{(i-1)}$$

$$+ h^{(i)}\rho^{(i)}\omega^2 \bar{D}_{3mn}^{(i)} = 0, \quad (22)$$

where R_{mnp}, Q_{mnp} and P_{mnp} are linear functions of $F_{\alpha mnp}$ and $F_{\alpha mnp,3}$, and $\tilde{V}^{(i)}$ is a function of x_1 and x_2. The continuity conditions $(8)_{3,4}$ at the interface between the plate and the actuator give the following.

$$\sum_{p=1}^{6} F_{1mnp}^{(i-1)}(h^{(i-1)}) D_{mnp}^{(i-1)} - \bar{D}_{1mn}^{(i)} = 0,$$

$$\sum_{p=1}^{6} F_{2mnp}^{(i-1)}(h^{(i-1)})D_{mnp}^{(i-1)} - \bar{D}_{2mn}^{(i)} = 0,$$

$$\sum_{p=1}^{6} F_{3mnp}^{(i-1)}(h^{(i-1)})D_{mnp}^{(i-1)} - \bar{D}_{3mn}^{(i)} = 0,$$

$$\sum_{p=1}^{6} F_{1mnp}^{(i+1)}(h^{(i)})D_{mnp}^{(i+1)} - \bar{D}_{1mn}^{(i)} = 0,$$

$$\sum_{p=1}^{6} F_{2mnp}^{(i+1)}(h^{(i)})D_{mnp}^{(i+1)} - \bar{D}_{2mn}^{(i)} = 0,$$

$$\sum_{p=1}^{6} F_{3mnp}^{(i+1)}(h^{(i)})D_{mnp}^{(i+1)} - \bar{D}_{3mn}^{(i)} = 0, \quad (23)$$

where coefficients $\bar{D}_{\alpha mn}^{(i)}$, $\alpha = 1, 2, 3$ are to be determined.

Solutions for sensor layers

Let the ith layer made of a PZT material act as a sensor. For it, we assume that the displacement field is given by (20), and

$$\Phi^{(i)} = \sum_{m,n=1}^{\infty} \phi_{mn}^{(i)} \sin \alpha_m x_1 \sin \beta_n x_2. \quad (24)$$

A procedure similar to that used for an actuator layer yields the following set of equations.

$$\sum_{p=1}^{6} R_{mnp}^{(i+1)}(h^{(i)})D_{mnp}^{(i+1)} - \sum_{p=1}^{6} R_{mnp}^{(i-1)}(h^{(i-1)})D_{mnp}^{(i-1)}$$

$$+h^{(i)}[\rho^{(i)}\omega^2 - c_{11}^{(i)}\alpha_m^2 - c_{66}^{(i)}\beta_n^2]D_{1mn}^{(i)}$$

$$-h^{(i)}(c_{12}^{(i)} + c_{66}^{(i)})\alpha_m\beta_n D_{2mn}^{(i)} + e_{31}^{(i)}\alpha_m\phi_{mn}^{(i)} = 0,$$

$$\sum_{p=1}^{6} Q_{mnp}^{(i+1)}(h^{(i)})D_{mnp}^{(i+1)} - \sum_{p=1}^{6} Q_{mnp}^{(i-1)}(h^{(i-1)})D_{mnp}^{(i-1)}$$

$$-h^{(i)}(c_{12}^{(i)} + c_{66}^{(i)})\alpha_m\beta_n D_{1mn}^{(i)}$$

$$+h^{(i)}[\rho^{(i)}\omega^2 - c_{66}^{(i)}\alpha_m^2 - c_{11}^{(i)}\beta_n^2]D_{2mn}^{(i)}$$

$$+ e_{31}^{(i)}\beta_n\phi_{mn}^{(i)} = 0,$$

$$\sum_{p=1}^{6} P_{mnp}^{(i+1)}(h^{(i)})D_{mnp}^{(i+1)} - \sum_{p=1}^{6} P_{mnp}^{(i-1)}(h^{(i-1)})D_{mnp}^{(i-1)}$$

$$+h^{(i)}(\rho^{(i)}\omega^2 D_{3mn}^{(i)} = 0. \quad (25)$$

Table 1. A comparison of the first six natural frequencies for a $30\sqrt{2} \times 30 \times 0.404$ cm simply-supported laminated plate as computed by the thin plate theory and the present analysis employing the three-dimensional linear elasticity theory

	Ω_{11}	Ω_{21}	Ω_{12}	Ω_{22}	Ω_{31}	Ω_{32}
Thin-plate theory	2.002	4.585	6.408	8.007	9.454	11.938
Present analysis (3-D theory)	1.944	4.456	6.152	7.736	9.128	11.528
% difference	3.0	2.6	4.0	3.3	3.5	3.0

The continuity conditions at the interface between a sensor and a laminate are analogous to eqn (23) with the addition of the following equation.

$$h^{(i)}e_{31}^{(i)}\alpha_m D_{1mn}^{(i)} + h^{(i)}e_{31}^{(i)}\beta_n D_{2mn}^{(i)} + \epsilon_{33}^{(i)}\phi_{mn}^{(i)} = 0. \quad (26)$$

Knowing ω and the voltage field applied to the actuators, we solve the aforestated equations for various Fourier coefficients and hence can find the displacements, stresses and sensor electric voltages at any point in the structure.

NUMERICAL RESULTS

As an example, we consider a $30\sqrt{2} \times 30 \times 0.404$ cm plate made of 10 layers of T300/976 graphite–epoxy laminates each 0.04 cm thick, a layer of PZT-G1195 actuator 0.002 cm thick, and a layer of PZT-G1195 sensor also 0.002 cm thick; the substrates are arranged symmetrically as 0/90/0/90. The material properties of the graphite/epoxy layer with respect to the principal axes of the load are taken to be

$$E_{11} = 150 \text{ GPa}, \quad E_{22} = E_{33} = 9 \text{ GPa},$$

$$\nu_{12} = \nu_{23} = \nu_{13} = 0.3,$$

$$G_{12} = G_{31} = 7.1 \text{ GPa}, \quad G_{23} = 2.5 \text{ GPa},$$

$$\rho = 1600 \text{ kgm}^{-3},$$

Table 2. A comparison of the first six natural frequencies for a $30\sqrt{2} \times 30 \times 4.04$ cm simply-supported laminated plate as computed by the thin plate theory and the present analysis employing the three-dimensional linear elasticity theory

	Ω_{11}	Ω_{21}	Ω_{12}	Ω_{22}	Ω_{31}	Ω_{32}
Thin-plate theory	1.975	4.570	6.284	7.900	9.444	11.858
Present analysis (3-D theory)	1.664	3.276	4.021	4.992	5.443	6.657
% difference	15.75	28.32	36.01	36.81	42.37	43.86

and those for the PZT-G1195 are

$$\rho = 7500\ \text{kg m}^{-3},\quad [e] = \begin{bmatrix} 0 & 0 & -2.1 \\ 0 & 0 & -2.1 \\ 0 & 0 & 9.5 \\ 0 & 9.2 & 0 \\ 9.2 & 0 & 0 \\ 0 & 0 & 0 \end{bmatrix}^{T} \text{cm}^{-2};$$

$$[c] = \begin{bmatrix} 148 & 76.2 & 74.2 & 0 & 0 & 0 \\ & 148 & 74.2 & 0 & 0 & 0 \\ & & 131 & 0 & 0 & 0 \\ & & & 25.4 & 0 & 0 \\ & & & & 25.4 & 0 \\ & & & & & 25.4 \end{bmatrix} \text{GPa}.$$

The applied voltage is a half sine function over a rectangular region of $a/10.5 \times b/10.5$ with a peak value of 200 volts and equals zero outside this region. This simulates finite size PZTs used in practice.

The Fourier series converges very fast; it takes 30 terms to compute displacements accurate to first 5 significant digits. However, computation of stresses involves the spatial gradients of the displacements and more terms are needed. Here we take 400 terms to evaluate strains and stresses.

Natural frequencies of the plate

The structure has a series of natural frequencies which can be ordered as ω_{mn}, $m, n = 1, 2, \ldots$. These are determined by plotting the vertical component of the deflection at the point $(a/4, b/4)$ as a function of the forcing frequency. The deflection becomes large at certain discrete values of the forcing frequency which signifies the resonance phenomenon; the natural frequencies so computed are listed in Table 1. The normalized natural frequencies Ω_{mn} of the structure, estimated from the thin plate theory, and with the inertia and rigidity of the piezoelectric layers neglected, are given by [22]

$$\Omega_{mn} \equiv \frac{\omega_{mn}}{\left(\frac{\pi^2}{a^2}\left(\frac{D_{11}}{2\rho h}\right)^{1/2}\right)}$$

$$= \left\{m^4 + 2\frac{D_{12} + 2D_{66}}{D_{11}} m^2 \left(\frac{a}{b} n\right)^2 + \frac{D_{22}}{D_{11}}\left(\frac{a}{b} n\right)^4\right\}^{1/2}$$

where $D_{\alpha\beta} = E_{\alpha\beta}(2h)^3/12(1 - \nu^2)$, $\alpha, \beta = 1, 2, 6$ is the flexural rigidity. As is clear from the values listed in Table 1, the maximum difference between the first six natural frequencies computed from the thin plate theory with no PZT layers and the present analysis employing the three-dimensional elasticity theory and considering the inertia and rigidity of the PZT layers is 4%. Thus for a thin plate with very thin piezoelectric films embedded in it, both theories give nearly identical values of the natural frequencies, and thin PZT films do not affect noticeably the dynamic response of the structure. Our approach will yield

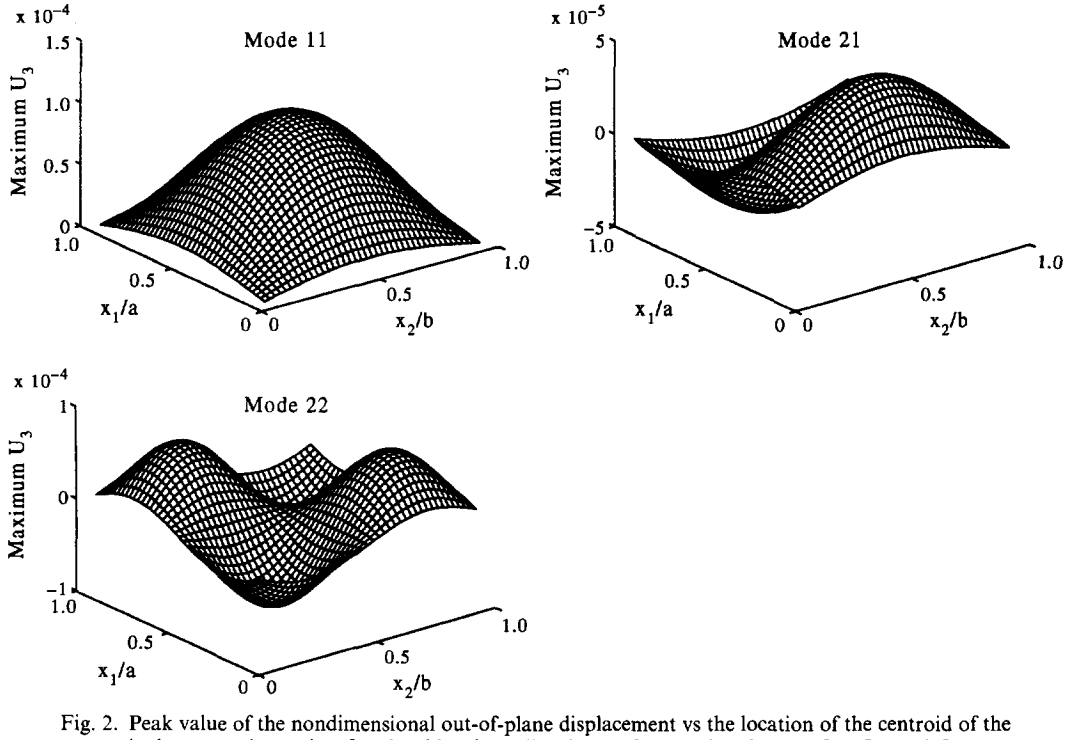

Fig. 2. Peak value of the nondimensional out-of-plane displacement vs the location of the centroid of the excited rectangular region for the thin plate vibrating at frequencies close to Ω_{11}, Ω_{21} and Ω_{22}.

good results for higher modes too and is valid for thick plates for which the thin plate theory may not yield satisfactory results. To demonstrate this, we have listed in Table 2 the first six natural frequencies for a $30\sqrt{2} \times 30 \times 4.04$ cm plate similar to the one considered above except that each lamina is 0.4 cm thick as computed by the present method and also by the thin plate theory; the maximum difference between the two sets of results is 44%.

The optimal placement of an actuator

An interesting exercise is to ascertain the optimal locations and sizes of actuators so that the energy is efficiently transferred to the structure (Bhargava *et al.* [1]). Such a problem is difficult to solve analytically. For the problem of the thin plate being studied herein, and as shown in the preceding section, the mass and rigidity of the piezoelectric layers have a negligible effect on the dynamic response of the structure. We find the optimal location of the actuator as follows. Let the thin PZT film cover the entire surface of the plate, and the voltage be applied only on a rectangular region of the surface. By fixing the applied voltage and the size of the excited region, we move the rectangular region around and find the maximum out-of-plane displacement of a point on the midsurface of the plate. The optimal location(s) of the excited region will be that which results in the maximum value of the peak out-of-plane displacement since if the plate were initially vibrating at the frequency of the applied voltage, such a location will be most effective in suppressing these vibrations with the least amplitude of the applied voltage. Here we delineate the optimal location for modes 11, 21 and 22.

Figure 2(a–c) depict the peak value of the nondimensional displacement $U_3 = u_3/a$ vs the location of the centroid of the excited region. It is evident that for the three modes studied the optimal location of the centroid of the excited region (and hence of an actuator patch of size equal to that of the excited rectangular region) coincides with the point(s) where the amplitude of vibration is maximum. Thus for modes 11, 21 and 22, the optimal locations of the centroid of the excited region are $(a/2, b/2)$; $(a/4, b/2)$ and $(3a/4, b/2)$; and $(a/4, b/4)$, $(a/4, 3b/4)$, $(3a/4, b/4)$ and $(3a/4, 3b/4)$, respectively. When the centroid of the excited region is located at a point on the nodal line consisting of points whose deflection for free vibrations of the plate is zero, the efficiency of actuation will be very poor.

Another part of the optimal placement of an actuator is to ascertain the optimal distance of the actuator layer from the neutral surface. Here we determine this for mode 11 and conjecture that the result will apply to higher modes too. We consider a laminated plate made of 20 substrate lamina arranged symmetrically as 0/90; the thickness of each substrate equals 0.2 mm and that of the PZT layer 0.01 mm. Keeping the centroid of the excited region at the

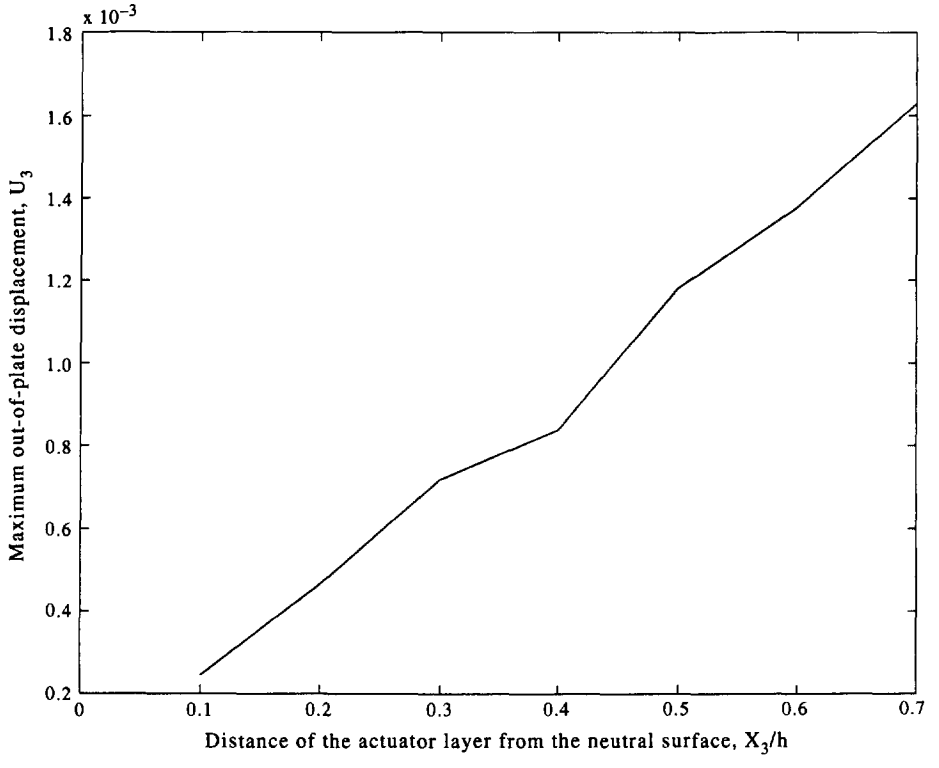

Fig. 3. Peak out-of-plane displacement vs the distance of the actuator layer from the neutral surface of the $30\sqrt{2} \times 30 \times 0.404$ cm plate.

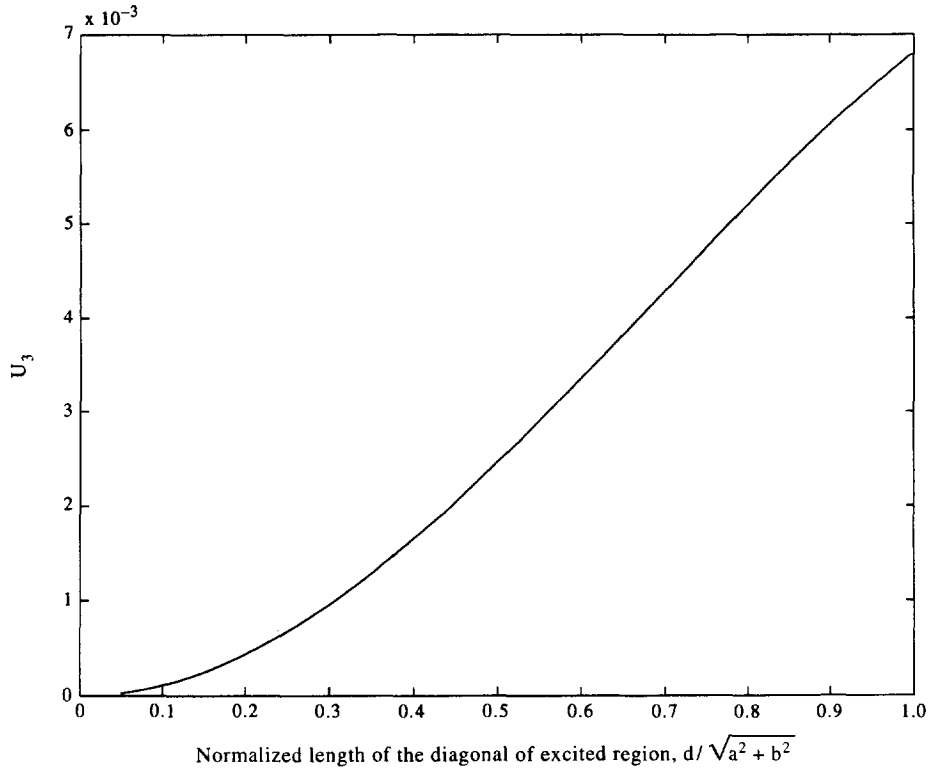

Fig. 4. Maximum out-of-plane displacement vs the length of the diagonal of the rectangular excited region for the $30\sqrt{2} \times 30 \times 0.404$ cm plate.

centroid of the plate, the size of the excited region as $a/10.5 \times b/10.5$ and the voltage applied to it fixed, we move the actuator layer in the x_3-direction. Recall that we also have a PZT layer used as a sensor that is located symmetrically with respect to the neutral surface. We note that displacements are very sensitive

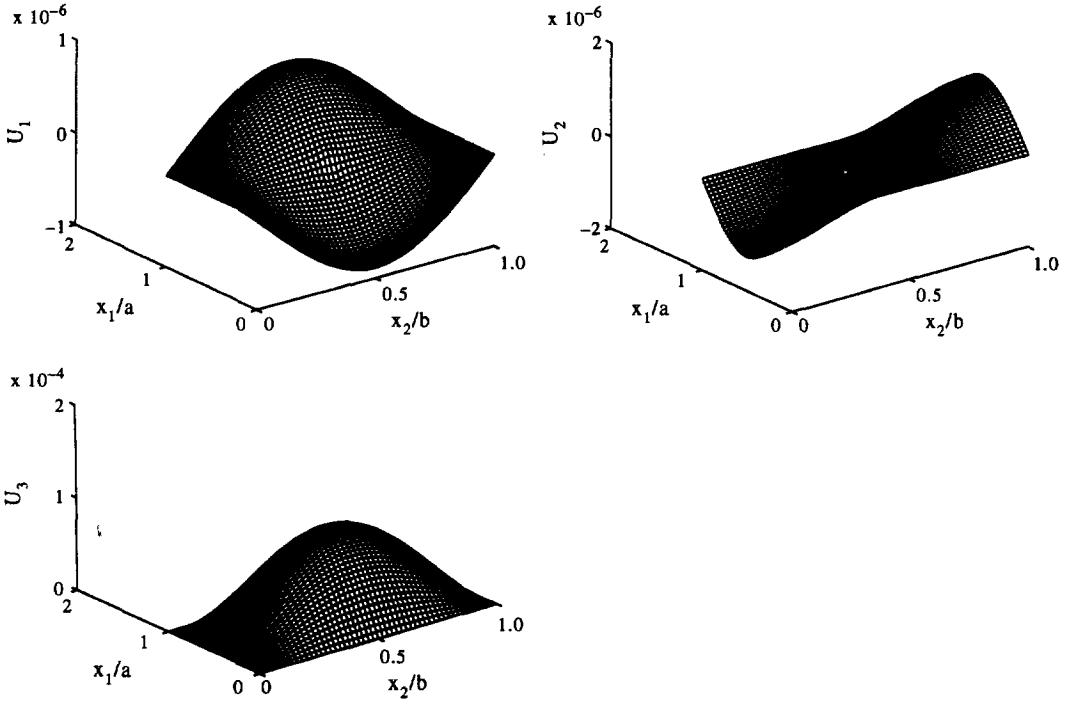

Fig. 5. Distribution of the non-dimensional displacements U_1, U_2 and U_3 for a thin plate vibrating at a frequency close to Ω_{11}.

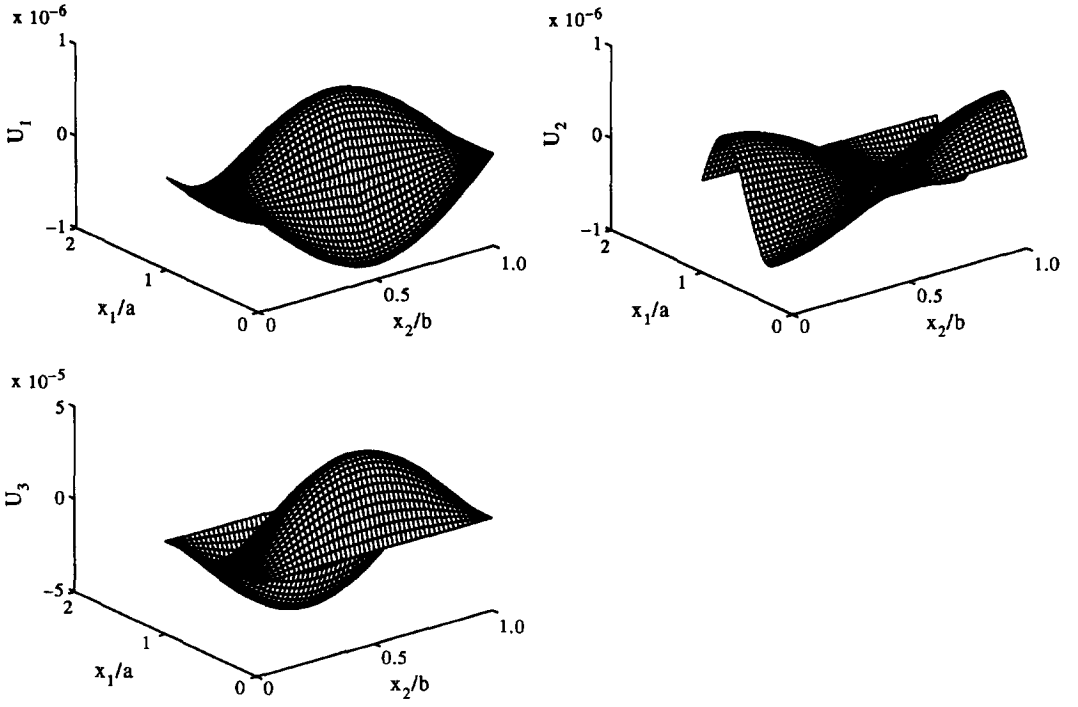

Fig. 6. Distribution of the non-dimensional displacements U_1, U_2 and U_3 for a thin plate vibrating at a frequency close to Ω_{21}.

to the frequency of the applied voltage when it is close to a natural frequency of the system, and Ω_{11} will vary slightly with the location of the actuator layer. In each case we take the non-dimensional frequency of the applied voltage to be 0.03 less than the corresponding Ω_{11}. As depicted in Fig. 3, the relation between the maximum out-of-plane displacement and the distance of the actuator layer from the neutral surface is essentially linear. Thus an optimum location for the actuator is at a bounding surface of

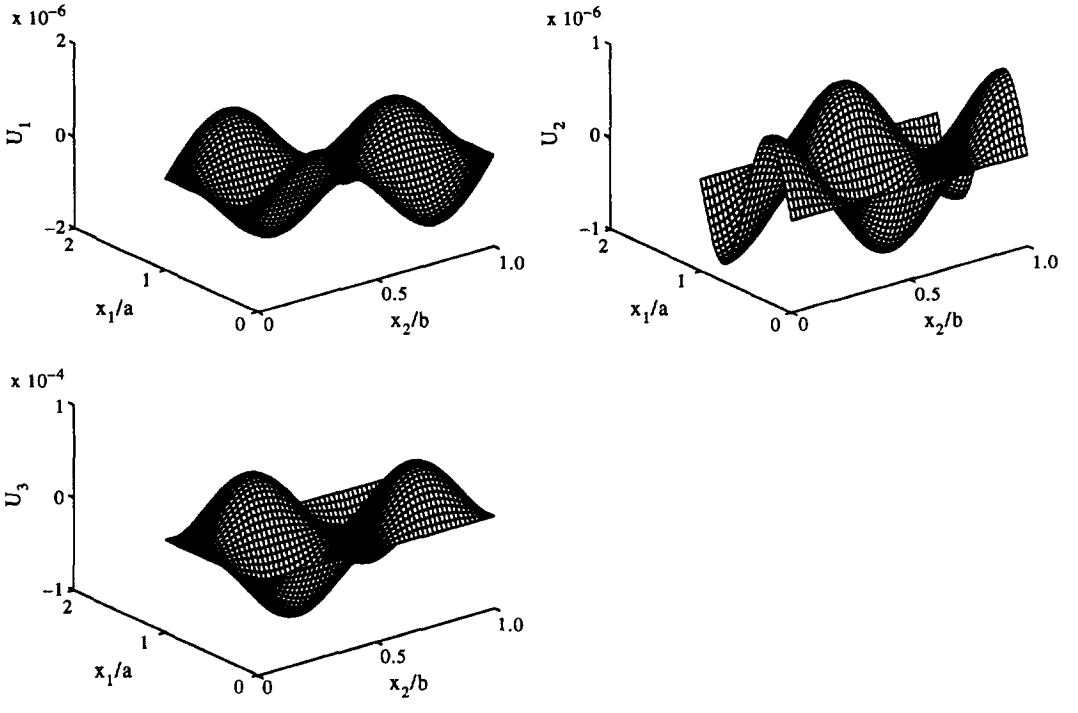

Fig. 7. Distribution of the non-dimensional displacements U_1, U_2 and U_3 for a thin plate vibrating at a frequency close to Ω_{22}.

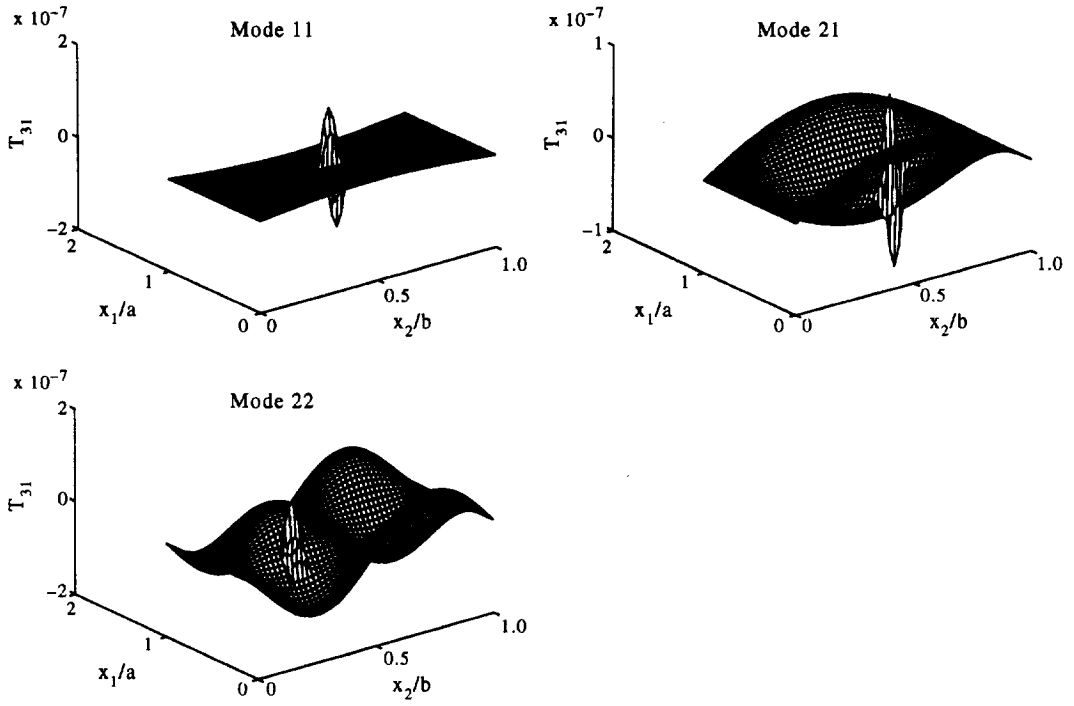

Fig. 8. Distribution of the non-dimensional shear stress T_{31} at the lower interface between the actuator and the substrate for a thin plate vibrating at frequencies close to Ω_{11}, Ω_{21} and Ω_{22}.

the plate. However, because of the assumption of embedded PZT layers, our analysis is not valid when the PZT layers are affixed to the top and bottom surfaces; those cases have been analyzed by Batra *et al.* [3]. Factors such as severe environment may suggest that it is better to have embedded PZTs.

For the $30\sqrt{2} \times 30 \times 0.404$ cm plate, Fig. 4 shows that the maximum out-of-plane displacement

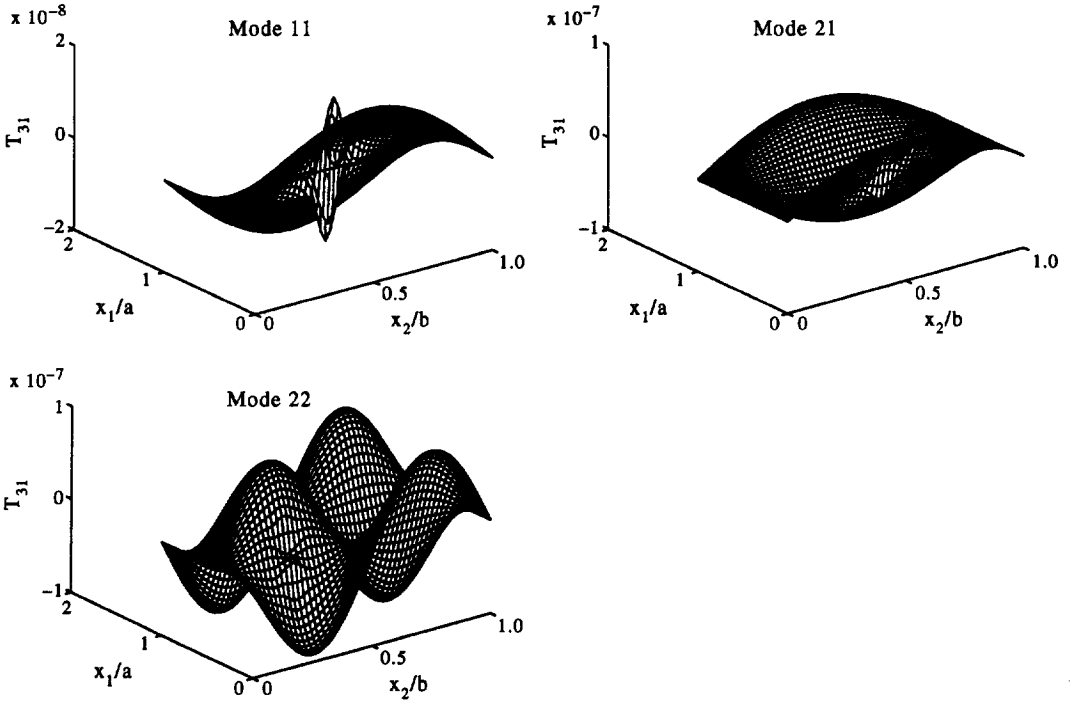

Fig. 9. Distribution of the non-dimensional shear stress T_{31} at the lower interface between the sensor and the substrate for a thin plate vibrating at frequencies close to Ω_{11}, Ω_{21} and Ω_{22}.

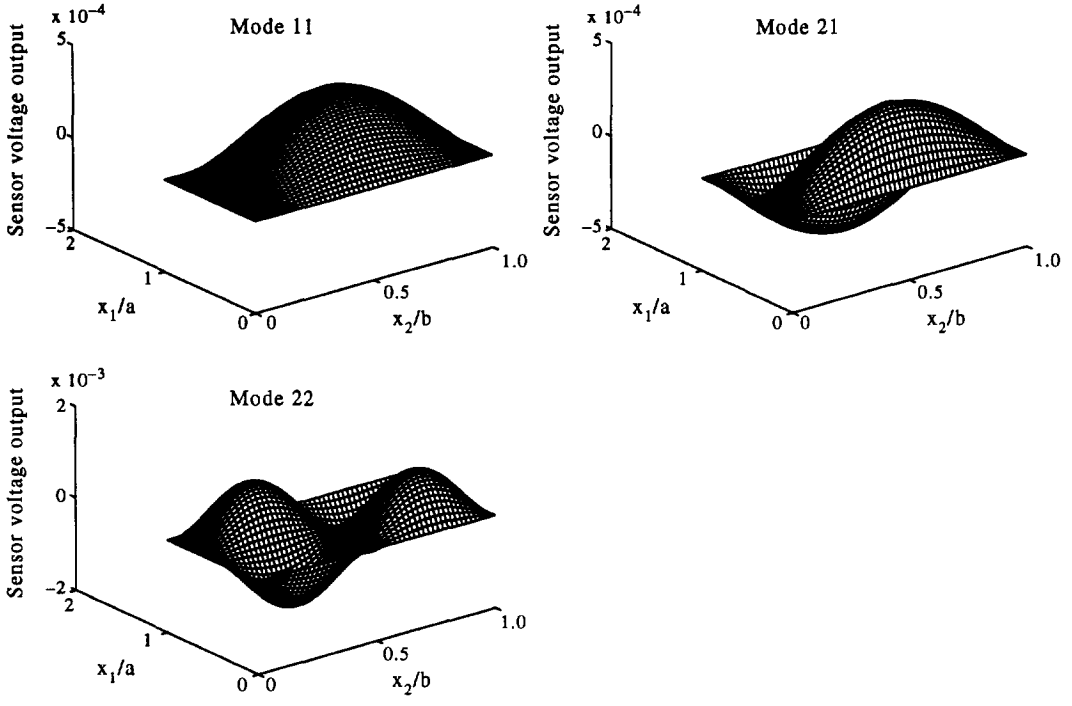

Fig. 10. Distribution of the normalized electric voltage $v/(200 \text{ volts})$ at the upper surface of the PZT sensor for a thin plate vibrating at frequencies close to Ω_{11}, Ω_{21} and Ω_{22}.

depends nonlinearly upon the size of the excited region. In each case the shape of the excited region, its centroid and the peak voltage applied with a frequency close to Ω_{11} are kept fixed. Since the applied voltage is a half sinusoidal wave, the resultant force and moment exerted by the forces between the actuator and the substrate layer depend nonlinearly upon the diagonal of the excited region.

Here we have kept the shape of the excited region as rectangular. Another possibility is to examine other shapes such as circular, elliptic, etc. and also consider variations in the distribution of the voltage applied to this region. However, these numerous investigations have not been carried out here. One difficulty with shapes of the excited region other than a rectangular one is the evaluation of the integrals in eqn (22). These can be evaluated analytically for a rectangular region. The evaluation of these integrals by a quadrature rule results in very high values of the shear stress at the quadrature points.

Structural response

In the laminated rectangular plate made up of 10 graphite–epoxy lamina and 2 PZT layers, we assume that 3rd and 10th layers from the bottom are made of a PZT and the former acts as a sensor and the latter as an actuator. The centroid of the excited region $(a/10.5, b/10.5)$ is located at $(a/2, b/2)$ for mode 11, $(a/4, b/2)$ for mode 21 and $(a/4, b/4)$ for mode 22 which were found to be optimal locations in the previous section. Figures 5–7 depict the distribution of the nondimensional displacement $U_\alpha = u_\alpha/a$ for modes 11, 21 and 22, respectively. It is clear that the magnitude of U_3 is about 100 times that of U_1 and U_2.

In order to check the integrity of the smart structure, we have plotted in Figs 8 and 9 the nondimensional shear stress $T_{31} = \tau_{31}/E_{11}$ at the lower interface between the actuator and the substrate, and at the lower interface between the sensor and the substrate. In the former case, the maximum shear stress occurs at a point in the excited rectangular region indicating the possibility of delamination there between the PZT layer and the substrate. Similar results were obtained by Hanagud and Kulkarni [23] for beams by the finite element method, for quasistatic deformations of plates by Zhou and Tiersten [17], and for steadily vibrating plates with no PZTs by Yang *et al.* [19]; Refs [17] and [19] used the elasticity theory. The magnitude of the maximum shear stress between the sensor and the substrate is about one-tenth that between the actuator and the substrate, and the jump in the shear stress at any point is also considerably smaller than that in the excited region of the actuator. For the sensor/substrate interface, the shear stress in the region that is below the excited region is high indicating the possibility of delamination there. However, the risk of this happening is lower than that in excited actuator region because of an order-of-magnitude difference in the magnitude of the maximum shear stress in the two cases.

For the plate vibrating in mode 11, 21 or 22, Fig. 10 depicts the output electric voltage at the upper surface of the sensor layer; in each case the point where the magnitude of the output voltage is maximum coincides with the point of peak out-of-plane displacement.

The variation in the x_3-direction at the point $(a/4, b/4)$ of nondimensional displacement components and stress components for the thin and thick plates studied herein and vibrating at a frequency close to Ω_{11} are shown in Figs 11 and 12. Both for the thin and the thick plates studied herein, U_1 and U_2 vary linearly through the thickness; however they are an order of magnitude higher for the thin plate as compared to that for the thick plate. The variation of U_3 through the thickness is parabolic for the thin and thick plates, but that for the thin plate is about 100 times that for the thick plate. The variation of different stress components in the thickness direction for the two plates is similar; as expected T_{11} and T_{22} exhibit discontinuities at the interfaces but other stress components are continuous as required by the coherency condition. Maximum values of T_{11}, T_{22} and T_{33} for the thin plate are nearly one-tenth of those for the thick plate; the peak values of other components of the stress tensor are essentially the same for the two plates.

CONCLUSIONS

We have studied steady-state vibrations of a simply-supported rectangular laminated elastic plate with embedded piezoelectric actuators and sensors by using the three-dimensional elasticity theory. The piezoelectric sensor and actuator layers are modeled as thin films and are assumed to be perfectly bonded to the adjoining lamina. Numerical results for a thin and thick plate are presented. For very thin sensor and actuator layers, the mass and rigidity of the PZT material have negligible effects on the natural frequencies of a laminated thin plate. For a thin plate vibrating at a frequency close to Ω_{11}, Ω_{21} and Ω_{22}, the optimal locations of the centroid of the excited rectangular region coincide with the points where the displacement for the corresponding mode attains maximum values. The shear stress in the excited region is high indicating the possibility of delamination there; however, the delamination will first occur at an interface between the actuator and the lamina rather than that between the sensor and the lamina. The points of maximum sensor output coincide with those of peak out-of-plane displacement. For the thin and thick plates, U_1 and U_2 vary nearly linearly with the distance from the midsurface, but U_3 varies parabolically.

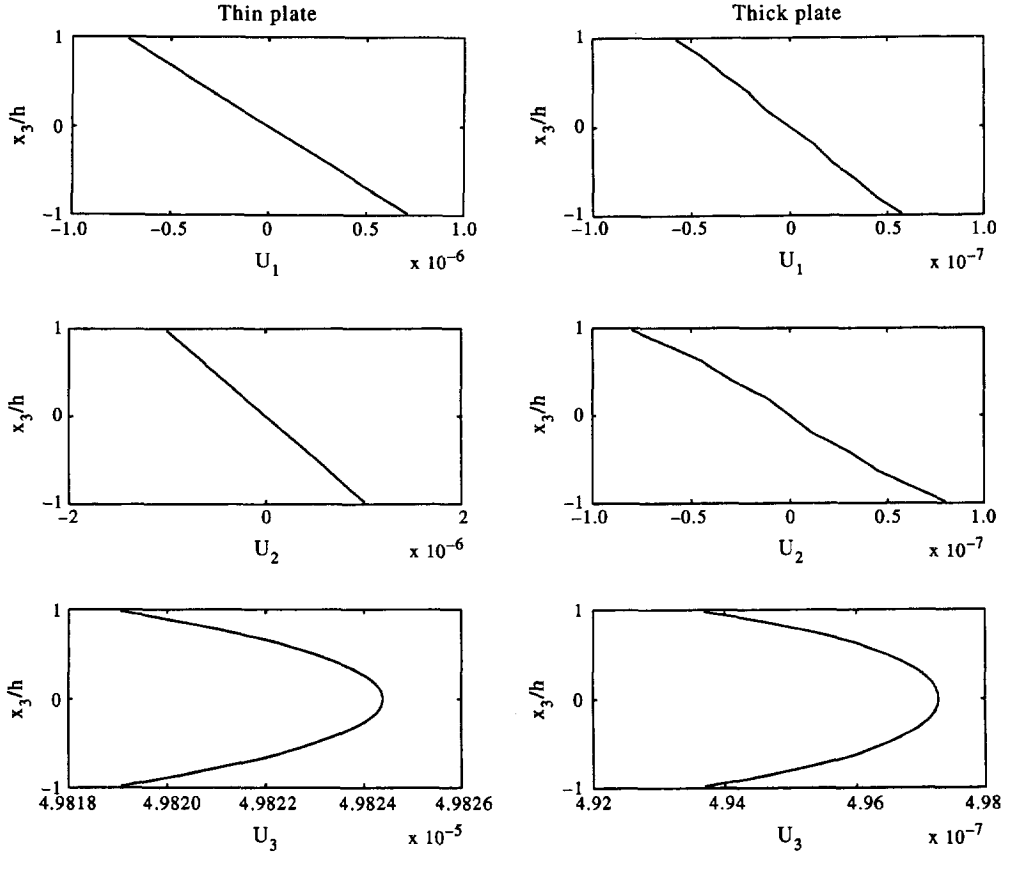

Fig. 11. Variations through the thickness of the non-dimensional displacement components at the point $(a/4, b/4)$ through the thickness for a thin and a thick plate vibrating at a frequency close to Ω_{11}.

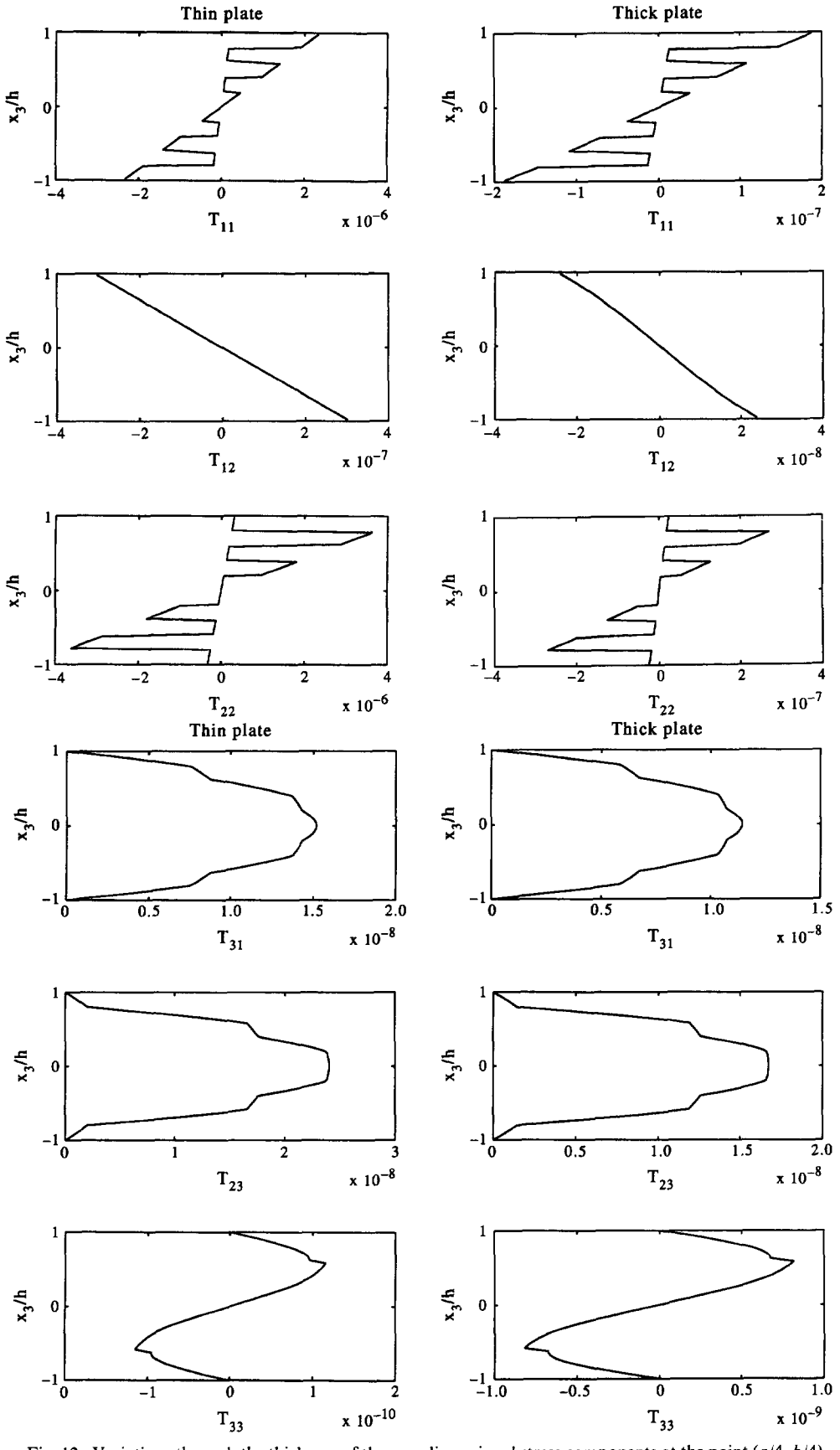

Fig. 12. Variations through the thickness of the non-dimensional stress components at the point $(a/4, b/4)$ for a thin and a thick plate vibrating at a frequency close to Ω_{11}.

Acknowledgements—This work was supported by the U.S. Army Research Office grant DAAH04-93-G-0214 to the University of Missouri-Rolla, and a matching grant from the Missouri Research and Training Center. The Virginia Polytechnic Institute and State University acted as a subcontractor to the University of Missouri-Rolla.

REFERENCES

1. A. Bhargava, Z. Chaudhry, C. Liang and A. C. Rogers, Experimental verification of optimum actuator location and configuration based on actuator power factor. *J. Intelligent Mater. Struct.* **6,** 411–418 (1995).
2. J. D'Cruz, Global multivariable vibration control and distributed piezoceramic actuators. *J. Intelligent Mater. Struct.* **6,** 419–429 (1995).
3. R. C. Batra, X. Q. Liang and J. S. Yang, Shape control of vibrating simply-supported rectangular plates. *AIAA J.* **134,** 116–122 (1996).
4. A. Baz and S. Poh, Performance of an active control system with piezoelectric actuators. *J. Sound Vibr.* **126,** 327–343 (1988).
5. H. S. Tzou and C. I. Tseng, Distributed modal identification and vibration control of continua: piezoelectric finite element formulation and analysis. *J. Dyn. Systems, Measurement Control* **113,** 501–505.
6. E. F. Crawley and J. de Luis, Use of piezoelectric actuators as elements of intelligent structures. *AIAA J.* **25,** 1373–1385 (1987).
7. T.R. Tauchert, Piezothermoelastic behavior of a laminated plate. *J. Thermal Stresses*, **15,** 25–37 (1992).
8. Y. Y. Tang and K. Xu, Dynamic analysis of piezothermoelastic laminate plate. *J. Thermal Stresses* **17** (1994).
9. J. A. Mitchell and J. N. Reddy, A refined hybrid plate theory for composite laminates with piezoelectric laminae. *Int. J. Solids Struct.* **32,** 2345–2368 (1995).
10. K. Ghosh and R. C. Batra, Shape control and plates using piezoceramic elements. *AIAA J.* **33,** 1354–1357 (1995).
11. R. C. Batra and K. Ghosh, Deflection control during dynamic deformations of a rectangular plate using piezoceramic elements. *AIAA J.* **33,** 1547–1548 (1995).
12. M. C. H. Ray, K. M. Rao and B. Samanta, Exact solution for static analysis of an intelligent structure under cylindrical bending. *Comput. Struct.* **47,** 1031–1042 (1993).
13. D. C. Lagoudas and Z. Bo, The cylindrical bending of composite plates with piezoelectric and SMA layers. *Smart Mater. Struct.* **3,** 309–317 (1994).
14. S. Brooks and P. Heyliger, Static behavior of piezoelectric laminates with distributed and patched actuators. *J. Intelligent Mater. Struct.* **5,** 635–646 (1994).
15. S. Srinivas, C. V. J. Rao and A. K. Rao, An exact analysis of vibration of simply supported homogeneous and laminated thick rectangular plates. *J. Sound Vibr.* **12,** 257–269 (1970).
16. W. H. Wittrick, Analytical, three-dimensional elasticity solutions to some plate problems, and some observations on Mindlin's plate theory. *Int. J. Solids Struct.* **23,** 441–464 (1987).
17. Y. S. Zhou and H. F. Tiersten, Elastic analysis of laminated composite plates in cylindrical bending due to piezoelectric actuators. *Smart Mater. Struct.* **3,** 225–265 (1994).
18. J. S. Yang, R. C. Batra and X. Q. Liang, The cylindrical bending vibration of a laminated elastic plate due to piezoelectric actuators. *Smart Mater. Struct.* **3,** 485–493 (1994).
19. J. S. Yang, R. C. Batra and X. Q. Liang, The vibration of a simply-supported rectangular elastic plate due to piezoelectric actuators. *Int. J. Solids Struct.* **33,** 1597–1618 (1996).
20. H. F. Tiersten, Electroelastic equations for electroded thin plates subject to large driving voltages. *J. Appl. Phys.* **74,** 3389–3393 (1993).
21. R. D. Mindlin, High frequency vibrations of plated crystal plates. *Progress in Applied Mechanics*, The Prager Anniversary Volume. MacMillan, New York, pp. 73–84 (1963).
22. R. M. Jones, *Mechanics of Composite Materials*. Scripta Book Co., Washington, D.C. (1975).
23. S. Hanagud and G. Kulkarni, Coupled piezoceramic-elastic structures with finite deformations. Developments in theoretical and applied mechanics. *Proc. 16th Southeastern Conf. on Theoretical and Applied Mechanics*, ed. B. Antar, R. Engels, A. A. Prinaris and T. H. Moulden, University of Tennessee Space Institute, Vol. XVI, pp. 22–30.